


Please cite the Published Version

Xue, Mi-An, Jiang, Zhouyu, Lin, Pengzhi, Zheng, Jinhai, Yuan, Xiaoli and Qian, Ling  (2021) Sloshing dynamics in cylindrical tank with porous layer under harmonic and seismic excitations. Ocean Engineering, 235. ISSN 0029-8018

DOI: <https://doi.org/10.1016/j.oceaneng.2021.109373>

Publisher: Elsevier BV

Version: Accepted Version

Downloaded from: <https://e-space.mmu.ac.uk/628070/>

Usage rights:  [Creative Commons: Attribution-Noncommercial-No Derivative Works 4.0](https://creativecommons.org/licenses/by-nc-nd/4.0/)

Additional Information: Author accepted manuscript published by and copyright Elsevier.

Enquiries:

If you have questions about this document, contact openresearch@mmu.ac.uk. Please include the URL of the record in e-space. If you believe that your, or a third party's rights have been compromised through this document please see our Take Down policy (available from <https://www.mmu.ac.uk/library/using-the-library/policies-and-guidelines>)

Sloshing dynamics in cylindrical tank with porous layer under harmonic and seismic excitations

Mi-An Xue ^{a,b,*}, Zhouyu Jiang ^{a,b}, Pengzhi Lin ^c, Jinhai Zheng ^{a,b}, Xiaoli Yuan ^d, Ling Qian ^{b,e}

^a Key Laboratory of Ministry of Education for Coastal Disaster and Protection, Hohai University, Nanjing 210024, China

^b College of Harbour Coastal and Offshore Engineering, Hohai University, Nanjing 210024, China

^c State Key Laboratory of Hydraulics and Mountain River Engineering, Sichuan University, Chengdu, 610065, China

^d College of Science, Hohai University, Nanjing 210024, China

^e Department of Computing and Mathematics, Manchester Metropolitan University, Manchester M1 5GD, United Kingdom

Abstract

The severe sloshing induced by earthquake in cylindrical liquefied petroleum gas (LPG) storage tank is of great concern for liquid storage design. For suppressing sloshing, porous material attached to inner periphery of the tank wall is proposed and studied numerically with the aid of OpenFOAM. The model was validated against with the available data of sloshing in cylindrical tank without and with ring baffle, and flow through porous media in a U-tube and porous dam break. Fair agreements between them are obtained. Findings show that damping effects of porous material was significant in linear sloshing scenario compared with ring baffle. The porous material layer was also proved to be good pressure absorber and energy dissipator as evidenced in pressure distribution and evolution of velocity and kinetic energy. Under 1-D harmonic excitation, nonlinear swirling waves could be effectively changed into planar waves due to the effects of porous material layer inside cylindrical tank. As a demonstration, sloshing damping effects of porous material layer in a real scale upright cylindrical tank under EL-centro earthquake excitation were investigated numerically.

1. Introduction

For preserving large volume of liquid fuel, cylindrical tanks are usually chosen as the ideal container shape for its simplicity in construction and its ability to withstand hydrodynamic pressure of the liquid. In spite of these advantages, under severe external excitations, e.g. earthquake, tsunami, cylindrical tanks can still face the danger of significant impact loads caused by nonlinear sloshing inside tank. Kang et al. (2019) numerically evaluated the nonlinear dynamic pressure acting on rigid cylindrical tank wall when being subjected to Imperial Valley, Kobe, and San Fernando earthquake excitations. Thus, damping the liquid sloshing inside cylindrical tanks itself is of paramount concern to engineers.

Many researchers focused on investigating the conditions under which a sloshing will be induced and the relationships between sloshing and external excitation by theoretical study and comprehensive model experiments. It is a general consensus that occurrence of sloshing largely depends on excitation conditions (Lin, 2007; Zhang et al., 2019b). Taking harmonic excitation as an example, amplitude and frequency need to be considered. The external excitation is also known

* Corresponding author.

E-mail address: coexue@hhu.edu.cn (M.-A. Xue)

as frequency offset in a mixed form according to Miles (1984),

$$\beta = \frac{\omega^2 - \omega_1^2}{\varepsilon^2 \omega_1^2}, \text{ where } \varepsilon^3 = 1.684 \frac{A}{R} \quad (1)$$

Where β is frequency-offset parameter, ε is a positive infinitesimal parameter, A is forcing amplitude (harmonic motion), R is radius of cylindrical tank. Based on this expression, external excitation can be determined exclusively by β . Miles introduced a list of values for β , which described the forcing conditions for inducing different types of sloshing waves.

Depending on frequency-offset value, three types wave regimes can be found in cylindrical tank sloshing, namely planar wave, swirling wave (rotary sloshing), chaotic wave. Comprehensive works on sloshing response in cylindrical tank under different excitation conditions have been widely carried out. In the scenario of 1-D horizontal harmonic linear excitation, 3-D swirling waves can be captured when excitation closes to resonant frequency. Systematic analyses of external forcing conditions for triggering swirling waves and relevant flow characteristics can be found in the works of Caron et al., 2018; Faller, 2001; Funakoshi and Inoue, 1988; Hutton, 1963; and Royon-Lebeaud et al., 2007. In fact, swirling wave is more common under rotatory excitation, as can be found in the variation of free surface when rotating a glass of wine. Scientifically, such rotating behavior can be expressed as orbital horizontal translatory excitation. Prandtl firstly carried out relevant experiments. For swirling wave, azimuthal mass transport (along with swirling wave propagating direction) is a noteworthy characteristic (also called Prandtl phenomenon, Prandtl, 1949), which results from the unbalance between tangential and normal fluid velocities (taking tank walls as references) when swirling wave is induced. For recent researches on Prandtl phenomenon see Bouvard et al. (2017) and Faltinsen and Timokha (2019). Also, liquid filling rate has positive or negative contribution to inducing resonant sloshing, i.e. ‘soft-spring’ and ‘hard-spring’ response (Chen and Xue, 2018; Waterhouse, 1994). Other than above mentioned parameters, liquid viscosity and surface tension, also affect the sloshing in containers.

Installing baffles inside tank, as a practical and efficient damping technique, has been commonly adopted in all kinds of engineering and investigated numerically and experimentally (Xue et al., 2013; 2017; 2019; 2020a). The corresponding free surface elevation and dynamic pressure on the tank wall are taken into consideration for evaluating the sloshing damping effects in baffled tanks under various fluid depths, forcing frequencies and amplitudes. Biswal et al. (2006) examined the position and size of baffles for damping sloshing in both rectangular and cylindrical tanks by finite element method. Xue and Lin (2011) investigated viscous liquid sloshing in 3-D rectangular tanks in different external excitations and dampening effects of ring baffles by developing 3-D numerical model NEWTANK (the updated version can be found in Lin et al., 2016). Their results of 3-D rectangular tanks with ring baffles induced by six degree-of-freedom excitation demonstrated good mitigating effects of ring baffles. Unal et al. (2019) researched numerically the damping effects of T-shaped baffles in a two-dimensional rectangular tank. They found a change of height of T-shaped baffles could either amplify or suppress the maximum surface height and this is related to the strength of vortices produced by both free surface and baffles. Akyldz et al. (2013) examined experimentally the damping effects of ring baffles and different arrangements of ring baffles in a cylindrical tank under pitch excitation.

Except installing rigid baffles inside tank, other novel methods were also proposed by researchers. Molin (2011) found that perforating parts of marine/offshore structures could be an efficient means in reducing inertia and slamming loads. Following this conclusion, Molin and Remy (2013) and Yu et al. (2019) proposed a new anti-sloshing device using perforated screen to mitigate undesirable sloshing. Koh et al. (2013) proposed a floating baffle constrained with cables to

suppress liquid sloshing in a rectangular tank. Similarly, Iranmanesh and Passandideh-Fard (2017) adopted a submerged cylinder hinged by spring-dampers in a 2-D rectangular tank to damp sloshing. Under constant acceleration and harmonic oscillatory excitation, the achieved suppression rate of total kinematic energy of entire fluid region indicated good mitigating effects of this method. Ning et al. (2019) and Zhang et al. (2019a), in their studies on using floating layers of foam for sloshing mitigation, showed that wave breaking in a rectangular tank can be suppressed by solid foam elements. Utilizing a high-density foam lid upon the free liquid surface, Hernandez-Hernandez et al. (2020) concluded that the non-planar sloshing in cylindrical tank can be suppressed effectively. Cho (2021) first proposed a flexible porous elastic baffle to reduce liquid sloshing in a rectangular tank. In this study, another innovative porous material layer damping sloshing method (Xue et al., 2020b) was proposed to study numerically its effectiveness in reducing sloshing in an upright cylindrical tank under harmonic and seismic excitations.

2. Mathematical model

2.1 Governing equations

The governing equations of two-phase incompressible flow combined with Volume of Fluid (VOF) method (Gomez-Goni et al., 2013; Hirt and Nichols, 1981) are as follows:

$$\frac{\partial u_i}{\partial x_i} = 0 \quad (2)$$

$$\frac{\partial \rho u_i}{\partial t} + \frac{\partial \rho u_j u_i}{\partial x_j} - \frac{\partial}{\partial x_j} (\tau_{ji}) = -\frac{\partial p}{\partial x_i} + \rho g_i + \sigma \kappa \frac{\partial \alpha}{\partial x_i} \quad (3)$$

$$\frac{\partial \alpha}{\partial t} + \frac{\partial u_i \alpha}{\partial x_i} = 0 \quad (4)$$

where σ is surface tension coefficient; κ is two-phase interface curvature; τ is shear stress; p is instantaneous effective pressure. The liquid of our study is water, in 25 °C, which surface tension σ is roughly 0.07 N/m² (Bond number $Bo = \frac{\rho g R^2}{\sigma} \approx 10^4$). Due to the minor effect of surface tension on sloshing wave, surface tension term will be omitted in momentum equation.

The description of porous flow depends on how to express the intrinsic friction effect of porous media. Based on this, Polubarinova-Kochina (1962) proposed a scheme of hydraulic gradient which describes the friction effect of porous media:

$$I = a_p \bar{u} + b_p |\bar{u}| \bar{u} + c_p \frac{\partial \bar{u}}{\partial t} \quad (5)$$

where the three coefficients a_p is linear drag coefficient (s/m), b_p is nonlinear drag coefficient (s²/m²), c_p is added mass coefficient (s²/m).

Van Gent (1995) conducted U-tube experiment with porous media placed inside tube to evaluate these coefficients values and relative magnitude of each term. Also, Van Gent developed numerical model on simulating composite breakwater equipped with porous layer under wave attack in 2-D scenario. It is noted that van Gent' model is targeted on solving large-scale wave propagation, which is based on shallow-water equation requiring some strict preconditions. For solving porous flow problems comprehensively, Hsu et al. (2002) presented Volume-Averaged/Reynolds Averaged Navier-Stokes (VARANS) combined with $k - \varepsilon$ turbulence model closure within the porous media, which modeled the flow outside and inside

porous media with the same equations. With the advantage of omitting the requirement of setting boundary condition at the interface between porous media and outside region, VARANS inherit the time averaging concept from RANS (Reynolds Averaged Navier-Stokes), using the volume averaging method to express the complex structure of porous media. Further, del Jesus et al. (2012) re-derived VARANS by optimizing some assumptions, allowing the porosity and pore diameters of porous media varying in space. With the derived governing form of VARANS, Higuera et al. (2014a, 2014b) developed numerical solver IHFOAM. The governing equations finally are derived as follows:

$$\frac{\partial}{\partial x_i} \left(\frac{\langle \bar{u}_i \rangle}{n} \right) = 0 \quad (6)$$

$$\begin{aligned} & \frac{1+c_A}{n} \frac{\partial \rho \langle \bar{u}_i \rangle}{\partial t} + \frac{\partial}{\partial x_j} \left(\rho \frac{\langle \bar{u}_j \rangle}{n} \frac{\langle \bar{u}_i \rangle}{n} \right) \\ &= -\frac{\partial}{\partial x_i} \left(\frac{\langle \bar{P} \rangle}{n} \right) + \rho g_i - \rho \frac{\partial \langle \bar{u}_i \bar{u}_j \rangle}{\partial x_j} + \frac{\partial}{\partial x_j} \left(\mu \frac{\partial}{\partial x_j} \frac{\langle \bar{u}_i \rangle}{n} \right) \\ & - \alpha_p \frac{(1-n)^3}{n^3} \frac{\mu}{D_{50}^2} \langle \bar{u}_i \rangle - \beta_p \frac{1-n}{n^4} \frac{\rho}{D_{50}} \langle \bar{u}_i \rangle |\langle \bar{u}_i \rangle| \end{aligned} \quad (7)$$

$$\frac{\partial \alpha}{\partial t} + \frac{\partial}{\partial x_i} \left(\alpha \frac{\langle \bar{u}_i \rangle}{n} \right) = 0 \quad (8)$$

where n is the porosity, D_{50} is the mean nominal diameter. α_p , β_p , c_A are the coefficients relating with Forchheimer coefficient a_p , b_p , c_p respectively, " $\langle \rangle$ " is Darcy's volume averaging operator, other symbols meanings are consistent with the terms in RANS.

2.2 Boundary condition

As the main considered boundary, the container wall is treated as non-slip boundary in our study. Numerically, no-slip boundary requires zero normal boundary flux, which can be satisfied by two conditions:

1. Velocity of the fluid at the wall is equal to the velocity of the wall.

$$\mathbf{u}_{fluid} = \mathbf{u}_{wall} \quad (9)$$

2. The shear stress exerted by the wall on the fluid is balanced with the fluid shear stress

$$\tau_{wall} = -\tau_{fluid} = -\mu \frac{\partial u_{\parallel}}{\partial x_{\perp}} \quad (10)$$

Where x_{\perp} is the normal distance from cell center to the boundary wall, u_{\parallel} is the fluid velocity component that tangential to the boundary wall (Fig. 1).

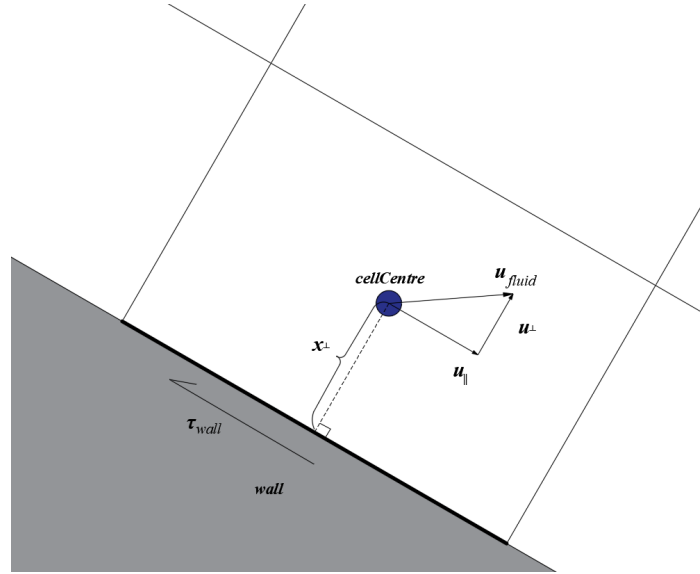


Fig. 1. A schematic of no-slip wall boundary condition

For free surface, OpenFOAM adopted VOF method to track free surface, which omits the process of setting pressure boundary on two-phase interface by letting water phase and air phase follow the same governing equations (Eq. 2-4). Analogously, the VARANS use volume-averaged strategy to couple clean fluid and porous layer region fluid in the same governing equations (Eq. 6-8), i.e. outside porous region, where porosity $n = 1$, VARANS is equal to RANS. Thus, there is no boundary setting need at the interface between fluid inside and outside the porous layer region.

3. Model validation

It is necessary to firstly validate the computing precision of IHFOAM. Therefore, this section is organized to validate numerical results computed by IHFOAM against the available data from literatures. Accordingly, first part will testify mesh convergence computed by IHFOAM and give a proper mesh size for latter computing; second part will verify surface elevation and kinetic response in a 3-D cylindrical tank in linear sloshing scenario; Furthermore, since cylindrical tank with ring baffle will be taken as a comparison case, third part will validate a ring-baffled tank case in terms of surface elevation features; Finally, Darcy seepage experiment in a U-tube and porous dam break cases are carried out numerically to verify the porous material model in IHFOAM. Important symbols are listed in Table 1.

Table 1 List of important symbols.

A	harmonic excitation amplitude
ω	angular frequency
H	tank height
H_l	water depth
R	cylindrical tank radius or ring baffle outer radius
R_l	ring baffle inner radius
h	ring baffle or pressure probe vertical height to tank bottom
η	free surface displacement
P_{dyn}	dynamic pressure
α_p	linear drag force coefficient
β_p	nonlinear drag force coefficient
c_A	inertial force coefficient
n	porosity
D_{50}	mean nominal diameter

3.1 Mesh convergence test

To choose an adequate mesh size for numerical computing on cylindrical tanks, three mesh scales, namely fine, normal and coarse mesh, are generated by GAMBIT. Geometric profile of cylindrical tank is presented in Fig. 2, where $R = H_1 = 0.508$ m, $H = 1$ m for convergence test. Tank wall is assumed to be rigid and impermeable, and subjected to horizontal harmonic motion ($x = A \sin(\omega t)$, $A = 0.002$ m, ω is set as the lowest natural frequency 5.8 rad/s which is determined by Eq. (11) as $k_{11}R = 1.841$). The free surface displacement near the rightest tank wall is measured (located at $x = R-r$, $y = 0$ with resolution $r = 0.005$ m).

$$\omega_{mn} = \sqrt{gk_{mn} \tanh(k_{mn}h)} \tag{11}$$

The details of mesh and computed results are presented in Table 2 and Fig. 3. It is noted that the free surface displacements computed by three meshes have no prominent discrepancy. But for coarse mesh, since the size of mesh unit near free surface is larger than other mesh case, the initial extracted surface height is not consistent with supposed height 0.508 m. In other two mesh cases, this initial error is not significant, which indicates the sizes of mesh unit have satisfied computing precision. Considering both computing precision and running time, normal mesh size is finally chosen for the following computing.

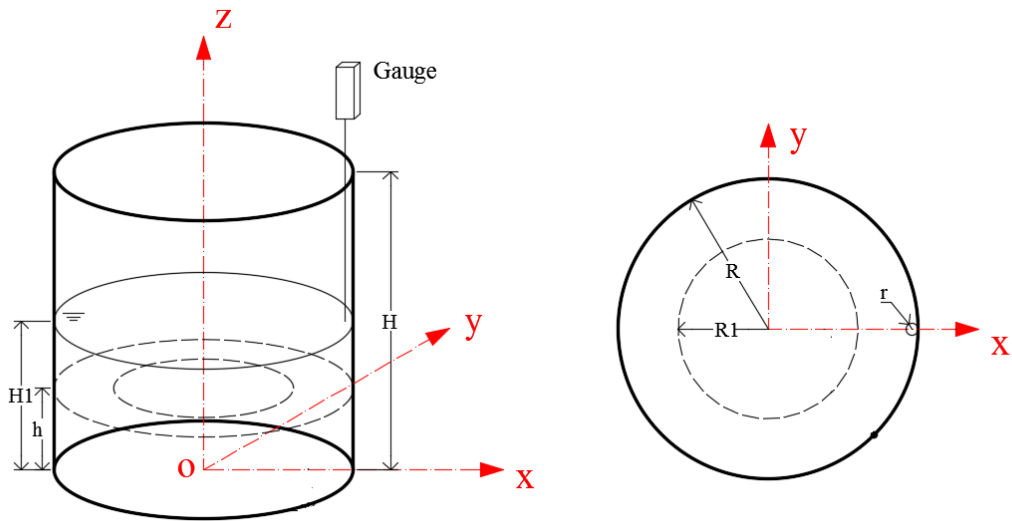


Fig. 2. Symbol definition of geometric characteristics in a cylindrical tank.

Table 2 Mesh details for mesh convergence test.

Grid description ($N_{xy} \times N_z$)	Mesh unit height near free surface (cm)	Extracted initial free surface height (m)	Simulation duration (s)	Running time (s)
2000×25 (coarse)	1	0.50322	15	10717
2000×50 (normal)	0.5	0.50859		19334
4500×100 (fine)	0.5	0.50828		87312
Computed by <i>Intel(R) Core i3-4160</i> .				

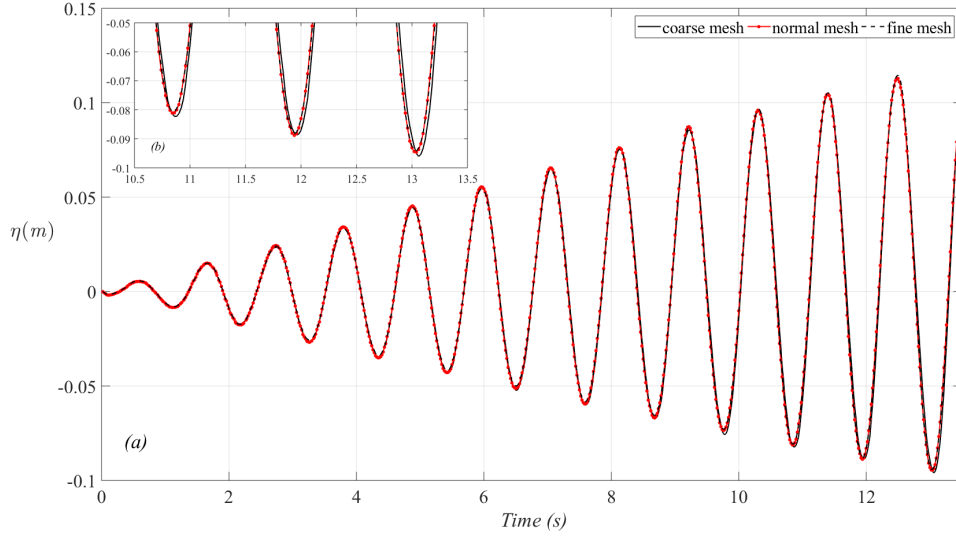


Fig. 3. Comparison of free surface displacement history near the right wall of three mesh scales, (b) is zoomed in from (a).

3.2 Sloshing in an unbaffled cylindrical tank

The free sloshing in a cylindrical tank is simulated in IHFOAM. Tank size is the same as the case of mesh convergence test, water height $H_1 = R = 0.508$ m. External excitation is followed as horizontal harmonic motion $x = A \sin(\omega t)$, $A = 0.002$ m, $\omega = 5.5$ rad/s. A free surface elevation probe is located at the right tank wall (R, 0) with the extraction range radius $r = 0.005$ m. The free surface displacement history is compared against the data from Biswal et al. (2006), as shown in Fig. 4. A little phase difference is found at the end of the simulation due to considering effect of fluid viscosity in present numerical results. Overall, present results are in good agreements with the data from Biswal et al. (2006).

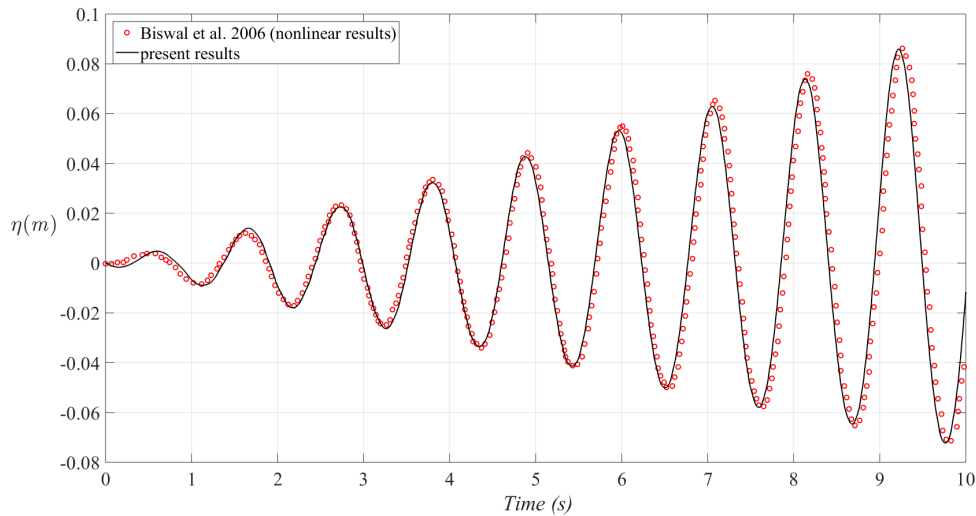


Fig. 4. Comparison of free surface displacement history in an unbaffled cylindrical tank between present results and data from Biswal et al. (2006).

Another case of sloshing in an unbaffled cylindrical tank with $H_1 = 2R = 2$ m, is simulated to examine force and moment acting on tank surrounding wall (kinetic response). The tank is under horizontal harmonic motion, $x = A \sin(\omega t)$, where $A = 0.0024$ m, $\omega = \omega_{11} = 4.2465$ rad/s. The steady-state results are compared with the data referred from Liang et al. (2020), as shown in Fig.

5. Fair agreements are obtained.

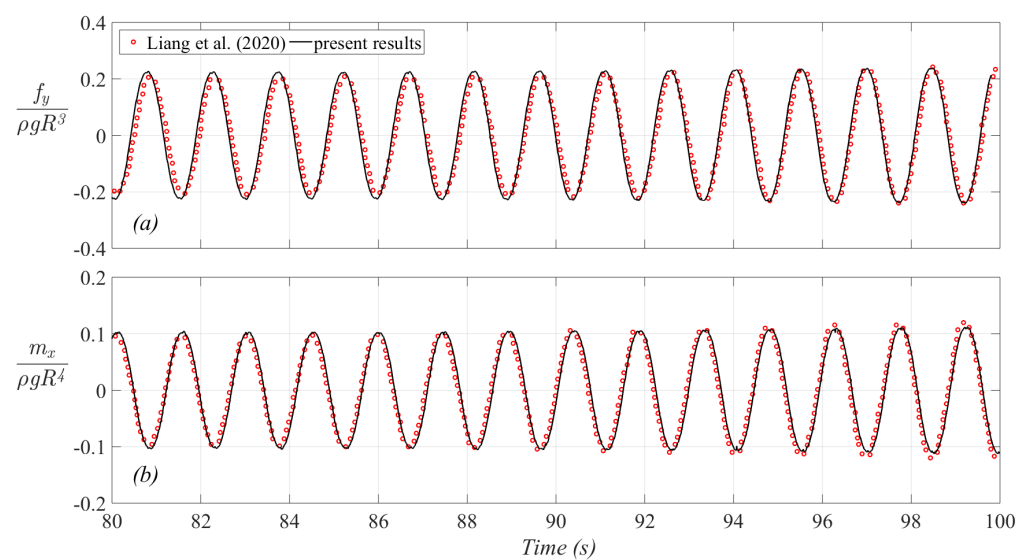


Fig. 5. Comparison of force and moment acting on surrounding tank wall between present results and data from Liang et al. (2020), where moment takes the center of initial free surface as reference point.

3.3 Sloshing in a baffled cylindrical tank

Biswal et al. (2006) concluded that the dampening effect of ring baffle increases when the vertical distance between ring baffle and liquid free surface decreases. To examine this conclusion, two different vertical location of ring baffle cases are simulated, where $h/H_1 = 0.2, 0.7$, R_1/R keeps constant as 0.6. In view of the thickness of baffle is usually unconsidered, the physical property of ring baffle is numerically attached to the faces of corresponding mesh units. Therefore, thickness of baffle is tiny, as shown in Fig. 6. Same size of cylindrical tank is chosen, where $H_1 = R = 0.508$ m, $H = 1$ m. External excitation keeps as horizontal harmonic motion $x = A \sin(\omega t)$ with $A = 0.002$ m and $\omega = 5.8$ rad/s. The free surface displacement at the right wall is measured.

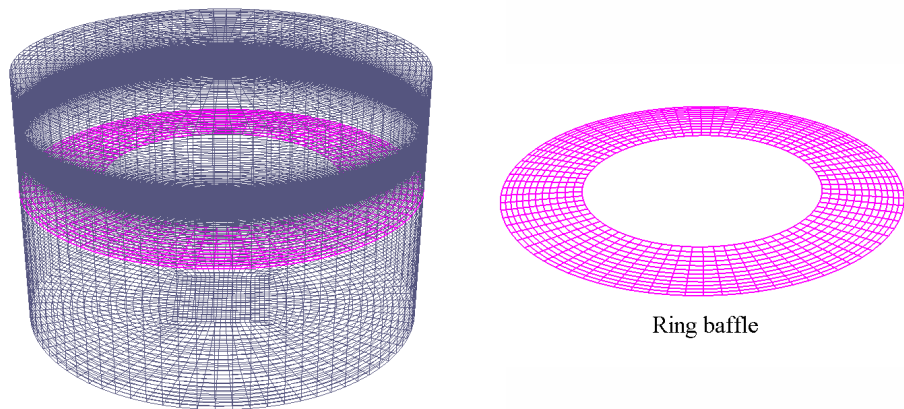


Fig. 6. Mesh of an upright cylindrical tank with ring baffle (highlighted by pink color).

Fig. 7 shows the comparison of free surface displacement history in a baffled cylindrical tank between present results and data from Biswal et al. (2006). For $h/H_1 = 0.7$, the amplitude response stops being amplifying after 4th period (4 s), while the amplitude of case $h/H_1 = 0.2$ is continuing to increase after that moment, which is similar to the trend of free sloshing case. Two cases verify

the conclusion that baffle closer to free liquid surface is more effective on dampening sloshing amplitude. Except minor discrepancy at the end of simulated time which might due to too small fluctuation amplitude, present results are in good consistence with the data from Biswal et al. (2006).

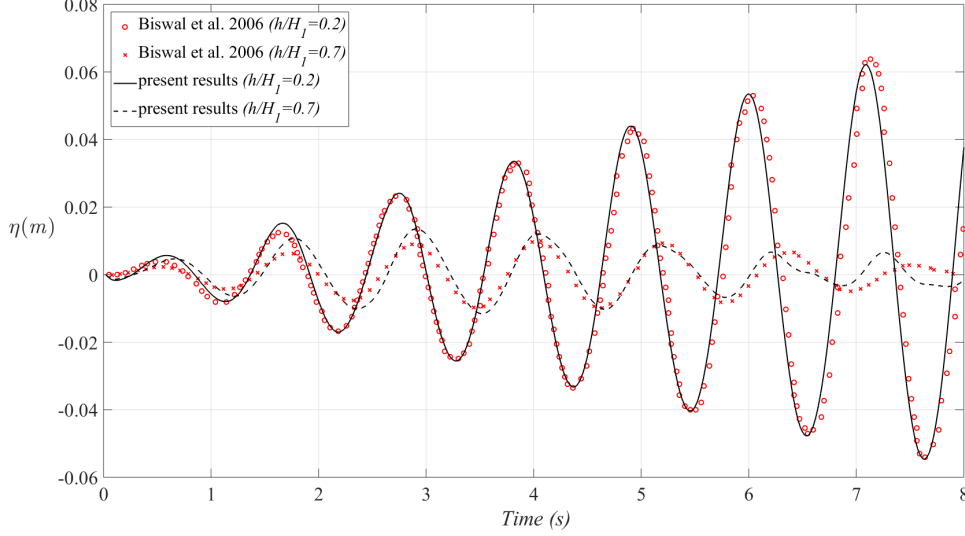


Fig. 7. Comparison of free surface displacement history in a baffled cylindrical tank between present results and data from Biswal et al. (2006).

3.4 Flow through porous media in a U-tube

The resistance force brought by porous media is important for simulating porous flow. To our best knowledge, there is no general formula on calculating resistance force, which might due to the complexity of porous media flow. According to previous studies (Higuera et al., 2014a; Hsu et al., 2002; Liu et al., 1999; Peng et al., 2017), resistance force is usually expressed by a linear combination of linear and quadratic part in terms of flow velocity. Meanwhile, some empirical parameters are introduced in and needed to be evaluated additionally. Focusing on the theme of this study, a general set of empirical parameter values are employed in this study, which are $\alpha_p = 200$, $\beta_p = 1.1$, $c_A = 0.34$. The Reynolds number inside porous media is defined as: $Re_p = \frac{|\bar{u}|D_{50}}{nv}$, it is often assumed when $Re_p > 60$, the quadratic term becomes important and turbulence should be considered additionally.

To validate the employed model for porous flow, Darcy seepage experiment is conducted numerically, where fluid flows through a region of porous material under gravity in a U-tube. The profile of this model is showed in Fig. 8. Assuming hydraulic gradient is always linear with flow velocity, the variance of two side water level differences in terms of time can be expressed by theoretical formula as:

$$\Delta H = \frac{\Delta H_0}{\exp(2K_h t / L)} \quad (12)$$

where ΔH_0 is initial water level difference between two side tube, K_h is hydraulic gradient (m/s), L is seepage path length through porous media (1 m).

Considering the assumption of Darcy seepage theorem, the quadratic and added mass terms are both neglected in this case (laminar regime). Three groups of linear drag term α_p are chosen as 200, 1000, 10000 respectively. About other properties of porous media, porosity is taken as uniform 0.4 in porous media region, characteristic diameters D_{50} is 4 mm according to the

relation of $K_h = \frac{\rho g K}{\mu}$ with $K = \frac{n^3 D_{50}^2}{150(1-n)^2}$ according to Peng et al. (2017). Whole computing region is divided by $0.04 \text{ m} \times 0.04 \text{ m}$ uniform grid.

Fig. 9 shows the comparison of free surface difference between analytical solution and numerical results. It is noted that when $\alpha_p = 1000$, good agreement is obtained, while in other two cases large inconsistency occurs, which reflects the α_p setting is critical. However, in high Reynolds situation, linear term is less important and $\alpha_p = 1000$ might not be as effective as this case (Van Gent, 1995). Here, it is recommended to set $\alpha_p = 1000$ in purely linear porous flow.

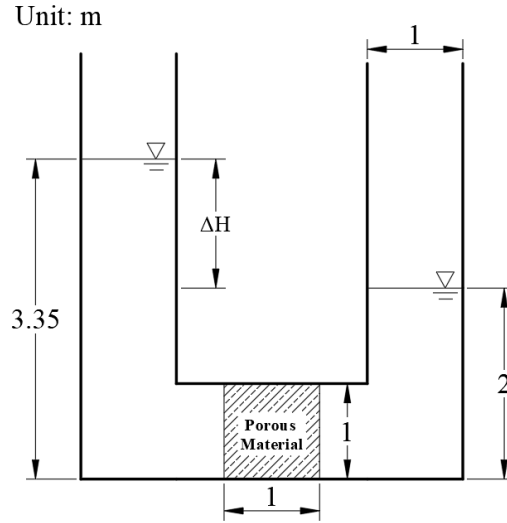


Fig. 8. Geometrical profile of Darcy seepage experiment.

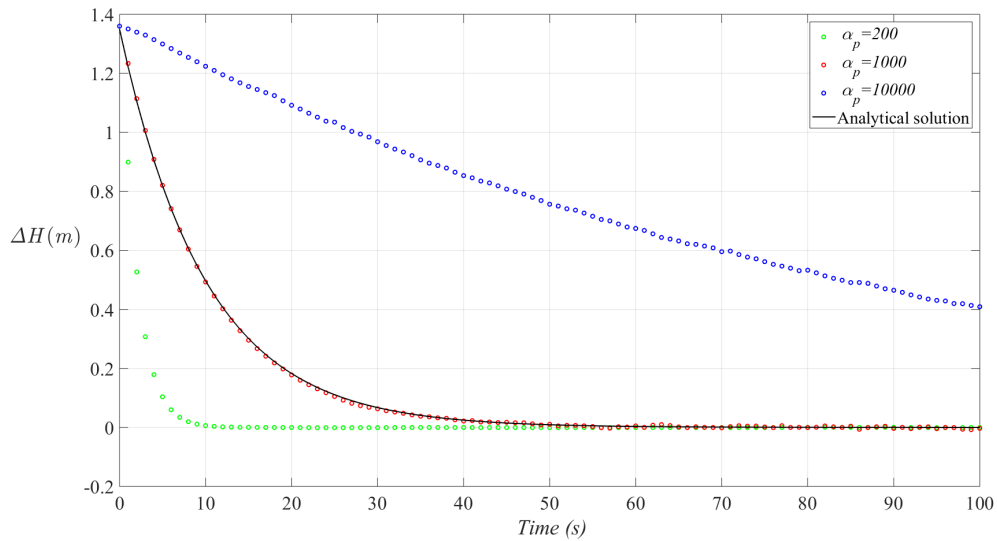


Fig. 9. Comparison of free surface difference time series between analytical solution and numerical results.

3.5 Porous dam break

A porous dam break validation case is conducted here, where a rectangular porous region is set at the middle area of a 2-D tank. By elevating water attitude at one side as initial condition, a break dam with flowing through porous media is investigated.

Tank is of rectangular shape with 0.89 m long, 0.58 m high. A rectangular porous zone is installed at the middle area with 0.29 m long (from location 0.30 m to 0.59 m) and 0.37 m high, separating the tank into two sides. The based water depth is 0.025 m. Initial left side elevated water rectangular zone is 0.28 m long and 0.25 m high (0.02 m horizontally away from left side of

porous media). Porous media consists of rocks ($n = 0.49$, $D_{50} = 0.0159$ m). In this case, because flow is more intense than Darcy's seepage experiment, nonlinear drag term and added mass term are needed to consider. Forchheimer empirical coefficients are set as $\alpha_p = 200$, $\beta_p = 1.1$, $c_A = 0.34$. Uniform mesh system (0.005 m long \times 0.0025 m high) is chosen to divide whole computational region. Computing time is set as 4 s. The free surface elevation of whole tank is taken as comparison (Fig. 10). At chosen instants, the free surface inside porous media reaches good agreement with experimental results.

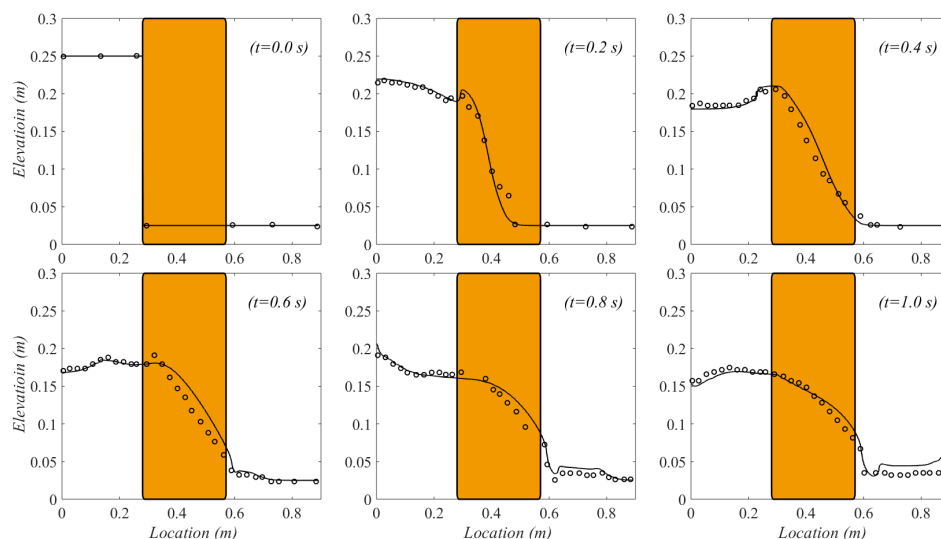


Fig. 10. Comparison of free surface elevation in typical instants, solid line is present results, circle is experimental results in Liu et al. (1999), brown region is porous media.

4 Effect of porous layer on sloshing dampening under harmonic excitation

Ye et al. (2018) researched the interaction between liquid and porous media in a cylindrical tank with scaled boundary finite element method. Their results presented the good dampening effect of porous media during liquid sloshing. Following their idea, the investigation on sloshing response in cylindrical tanks equipped with porous media is carried out in terms of pressure fluctuation history and pressure distribution along tank wall.

4.1 Problem descriptions

The cylindrical tank chosen from Haroun (1983) describes a water storage tank in the charge of the Metropolitan Water District of Southern California, as shown in Fig. 11. The tank rests on 3.66 m depth compacted gravel foundation, assuming there is no relative displacement between tank and foundation.

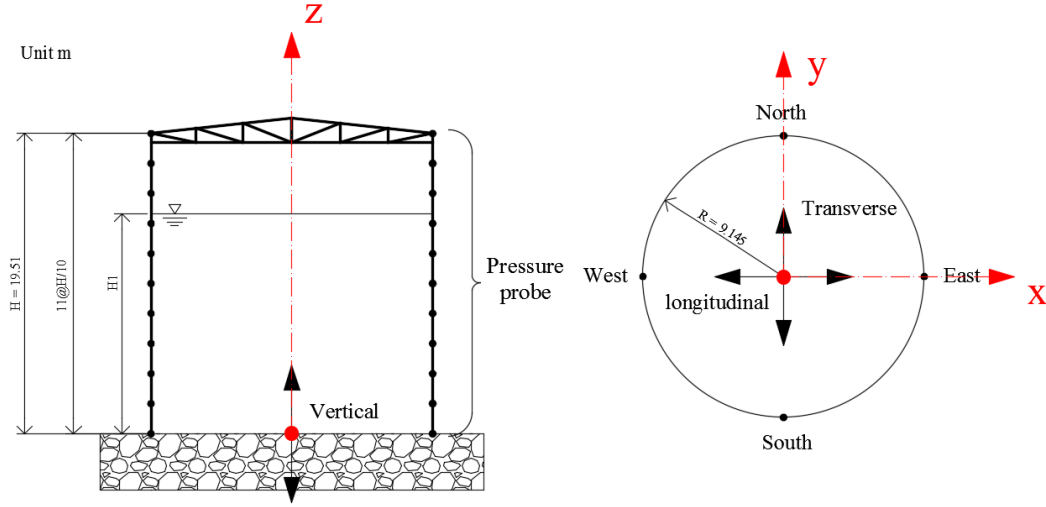


Fig. 11. Geometric profile of a real storage tank and definition of external motions (red circle indicates origin point).

To initially testify the effect of porous layer, reduced scale ratio of 1/20 is adopted to this rigid tank. The size of scaled-down tank ($R = 0.45725$ m, $H = 0.9755$ m) is closed to our foregoing model in mesh convergence test. The previous mesh scale 2000×50 , namely 'normal', is qualified to be employed here. Liquid filling ratio $H_1/H = 0.5$, external excitation is kept as horizontal harmonic motion $y = A \sin(\omega t)$ with $A = 0.002$ m and $\omega = \omega_1 = 6.16$ rad/s. As shown in Fig. 12, porous material layer is attached to inside walls of cylindrical tank to mitigate dynamic pressure acting on the cylindrical tank walls. In validation section, our numerical results fit well with Liu's experiment (i.e. $\alpha_p = 200$, $\beta_p = 1.1$, $c_A = 0.34$). Thus, three Forchheimer parameters of porous media are kept the same values as stated in Liu et al. (1999). Thickness, porosity and media diameter of porous material layer are determined according to the parameter optimizing results from our previous study (Xue et al., 2020b), which are $0.2R$, 0.51 , $0.02R$ respectively.

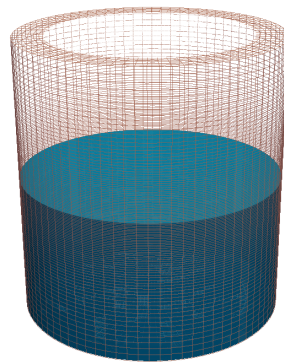


Fig. 12. Preview of half-loaded cylindrical tank with porous layer (highlighted by brown color).

4.2 Results and discussions

Pressure probes are embedded in cylindrical tank wall for obtaining sloshing pressure distribution acting on the tank walls. Meanwhile, liquid surface displacement near the right wall is also measured. Liquid sloshing in a cylindrical tank with ring baffle, where $h/H_1 = 0.7$, and $R_1/R =$

0.6, is also carried out to compare them with the results of sloshing interaction with porous layers.

Before presenting comparing results, it is necessary to demonstrate how many computing periods are suitable. About 500 sloshing periods for free sloshing case is firstly computed. The free surface displacement near tank wall is shown in Fig. 13. It is noted that before 165 wave periods sloshing wave height is irregular, accompanying with amplitude discrepancy between wave peak and trough (nonlinear characteristics). After 165 wave periods, steady-state sloshing wave is gradually established. In real engineering, transient sloshing response is of paramount concern. Also, considering saving computing time, 30 computing periods are finally chosen, which covers the occurrence of first maximum free surface displacement.

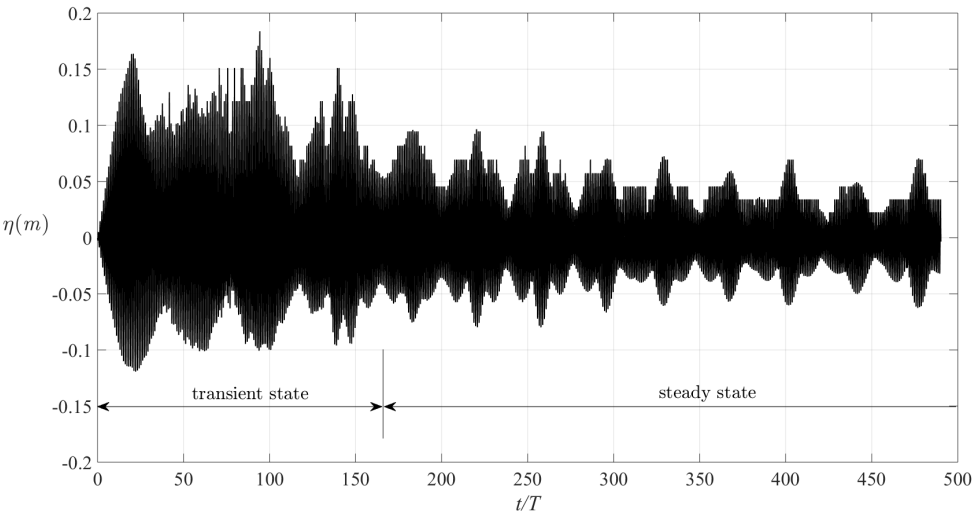


Fig. 13. Free surface displacement history near tank wall along excitation direction (0, *R*) about 500 periods, (free sloshing case, $T = \frac{2\pi}{\omega_1} \approx 1.02$ s).

As shown in Fig. 14, both free surface displacement and pressure fluctuation history exhibit good dampening effect of porous layer compared with ring baffles. With ring baffle or porous material layer, the free surface elevation or pressure responses are tended to reach steady state much quicker than free sloshing. After installing ring baffle or porous material layer, significant amplitude decay response is well captured in corresponding FFT analysis, where the dominant frequency component is only left with the lowest resonant frequency. The disappearance of higher resonant response frequency is related with the significant amplitude suppressing effect of porous material layer or ring baffles. To quantitatively evaluate the sloshing dampening effect, dampening rate is defined as D_r

$$D_r = \frac{\eta_{\max}^f - \eta_{\max}^d}{\eta_{\max}^f} \tag{13}$$

where η denotes the maximum free surface displacement or dynamic pressure, superscript f denotes free sloshing, d denotes sloshing with dampening device.

Table 3 Summary of damping rate comparisons.

	Free surface displacement	Dynamic pressure
Porous layer case	88.98%	74.04%
Ring baffle case	92.44%	91.20%

Damping rate results are shown in Table 3. For maximum free surface wave height, value of

D_r is 88.98% after attaching porous material layer to inner periphery of cylindrical tank wall and 92.44% after installing ring baffle inside cylindrical tank. For maximum dynamic pressure at tank bottom, the value of D_r is 74.04% for adopting porous material layer and 91.2% for adopting ring baffle. Although adopting porous material layer is not as effective as ring baffle, it is encouraged to see sloshing is mitigated by porous layer. In real engineering, installing ring baffle is prohibitive in LNG tank for stress concentration will occur at installing location (normally by welding). Adopting porous material, which has not changed the structure of tank wall, can be an alternative strategy. Thus, porous material layer is proved to be an effective device in sloshing mitigation design due to its advantage without requirement of welding compared with ring baffle.

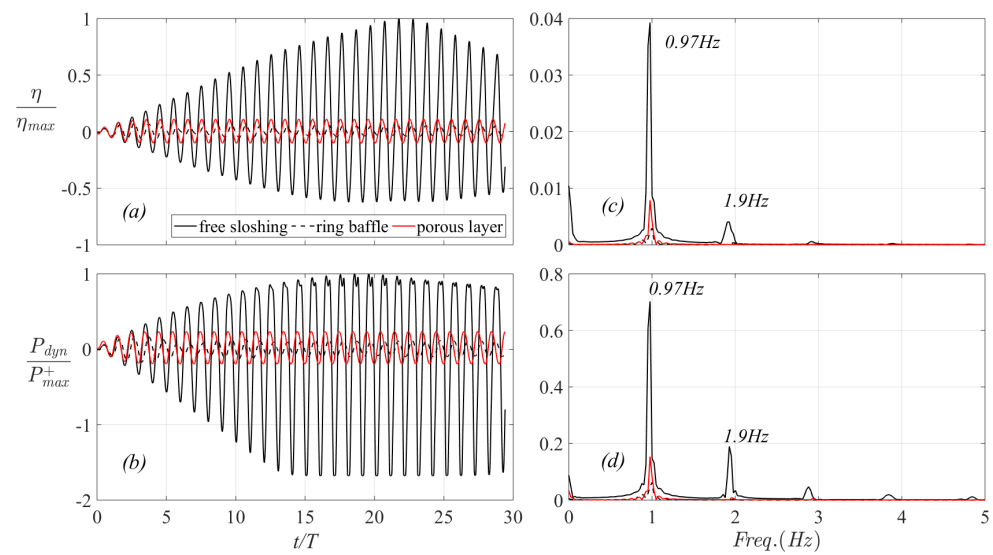


Fig. 14. (a) Comparison of water free surface displacement history near tank wall (0, R), $T = \frac{2\pi}{\omega_1} \approx 1.02$ s; (b) Comparison of dynamic pressure at tank bottom (0, R , 0); (c) Fast Fourier Transformation of (a); (d) Fast Fourier Transformation of (b).

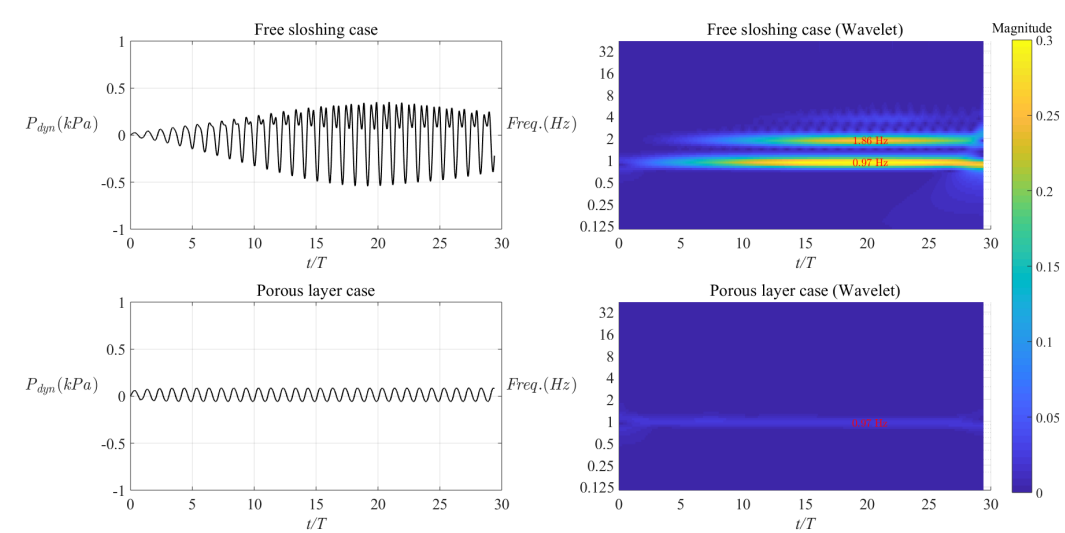


Fig. 15. Comparison of time history of dynamic pressure at free surface (0, R , H_l) (left column) and corresponding wavelet transform results (right column), the magnitude denotes wavelet coefficients (dimensionless), equal to amplitude in time domain.

The significant sloshing-induced dynamic pressure characteristics can be also found in Fig. 15, where in free sloshing case, pressure response exhibits strong nonlinearity after 4-5 periods,

and a double-peak pressure jet occurs at every peak after 10th period. Corresponding wavelet transform diagram tells this double-peak pressure jet consists of high order signal component (1.86 Hz). In porous material layer case, pressure response rapidly transforms to steady state with little fluctuation amplitude. The dominant wave ridge in wavelet transform result is only left with natural frequency ω_1 . Furthermore, the dynamic pressure distribution along the vertical direction of tank wall in four sides is investigated, as shown in Fig. 16. For free sloshing case, the dominant dynamic pressure occurs on the tank side parallel to excitation direction (north & south). In both north and south sides, the maximum pressure increases with the increase of vertical height, and reaching the maximum when vertical height is closed to free surface, then decaying rapidly. Along x direction, which is perpendicular to moving direction, a minor maximum pressure is found. This is due to the nonlinear sloshing, indicating that 3-D swirling wave component has been induced. After adopting porous layer, the maximum pressures in all locations decline in different degrees. Particularly, in x direction of wall (east & west), the dynamic pressure is almost eliminated, which indicates that previous 3-D swirling wave has disappeared and transformed to 2-D planar wave. The effect of porous material on swirling wave response would be discussed later.

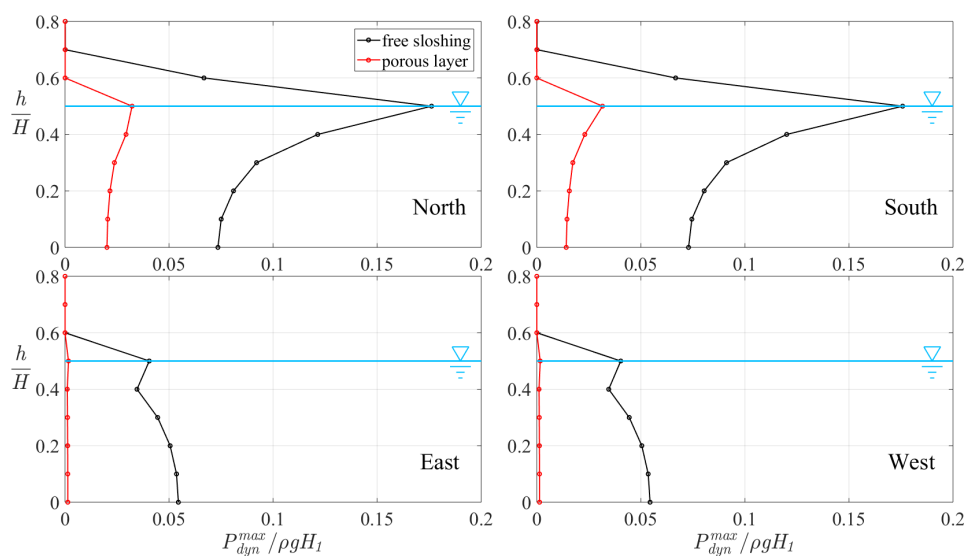


Fig. 16. Comparison of maximum dynamic pressure distribution on four sides wall under linear excitation, where $H_1 = 0.5H$.

Further, other than resonant frequency (0.98 Hz), a set of other excitation frequency cases are conducted for testing the dampening effect of porous material layer in different frequency range in linear sloshing scenario (keeping amplitude A still as 0.002). As a critical response characteristic, the maximum free surface displacement near tank wall ($0, R$) is chosen for comparing. The results (Fig. 17) show that in different frequency range porous material layer all exhibits sloshing dampening effect. It is noted that when sloshing response becomes more intense (frequency closed to resonant frequency), the dampening effect of porous material layer becomes more effective.

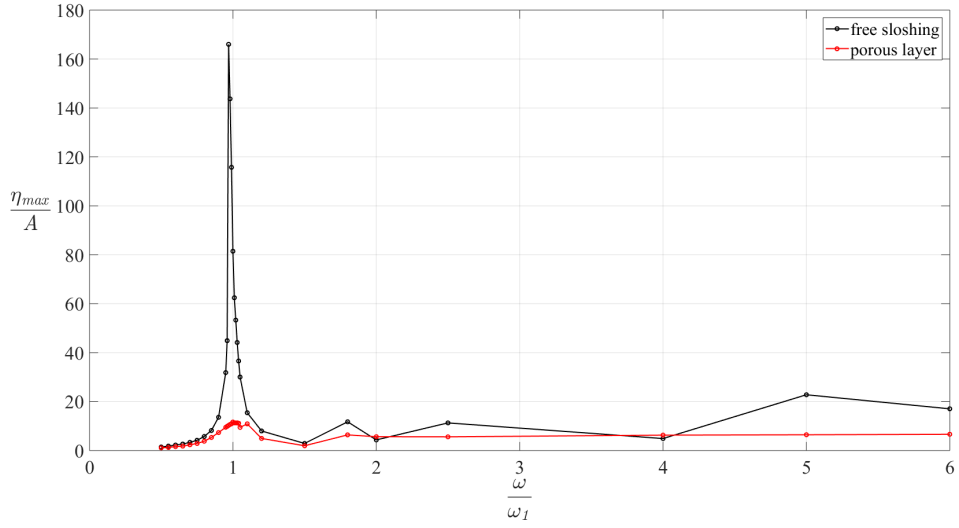


Fig. 17. Comparison of sloshing dampening effect of porous material layer in other frequency range in terms of maximum free surface displacement near tank wall (0, R).

4.3 Sloshing dampening analysis

Effects of ring porous material layer on dampening sloshing in cylindrical tank are proved to be effective. It is clear that the friction in porous material layer should play an important role on dampening sloshing. Considering the small amplitude linear sloshing case in the last part, the free surface displacement history obtained in Fig. 14 (a) indicates the significant of wave amplitude decay in porous layer case, or to say the loss of potential energy. To further clarify the energy dissipation, the kinetic energy distribution combined with velocity fields in small amplitude linear sloshing case is shown in Fig. 18, where free sloshing case is chosen from the most severe sloshing period and porous material layer case is chosen from the steady-state period. The kinetic energy value here has not multiplied fluid density and control volume, which are constant for both cases, so the comparison of kinetic energy value between two cases is still valid. From legend range, the maximum kinetic energy of porous layer case is far less than free sloshing case in any given time. When $t = 0, T/2, T$, at which potential energy is transformed to kinetic energy, the maximum kinetic energy of porous layer case ranges from 0.003 to 0.009, while the counterpart of free sloshing case reaches to 0.45-0.75.

Observing energy distribution at varied moment, for free sloshing case, primary kinetic energy distributes near free surface and comes to form two extremal areas when potential energy converts to kinetic energy. Furthermore, the relative larger extremal region is located at wave front. In porous layer case, kinetic energy still concentrates near free surface. However, primary kinetic energy is outside porous layer region, while inside porous layer no more significant kinetic energy occurs in any given time, indicating that the frictional function inside porous layer is remarkable. Except directly dissipating energy by porous layer intrinsic friction, a weak energy dissipation is found outside porous layer (red circle), where currents encounter face to face. This flow collision reflects phase lag in partial fluid area, which is also due to the effect of porous material layer.

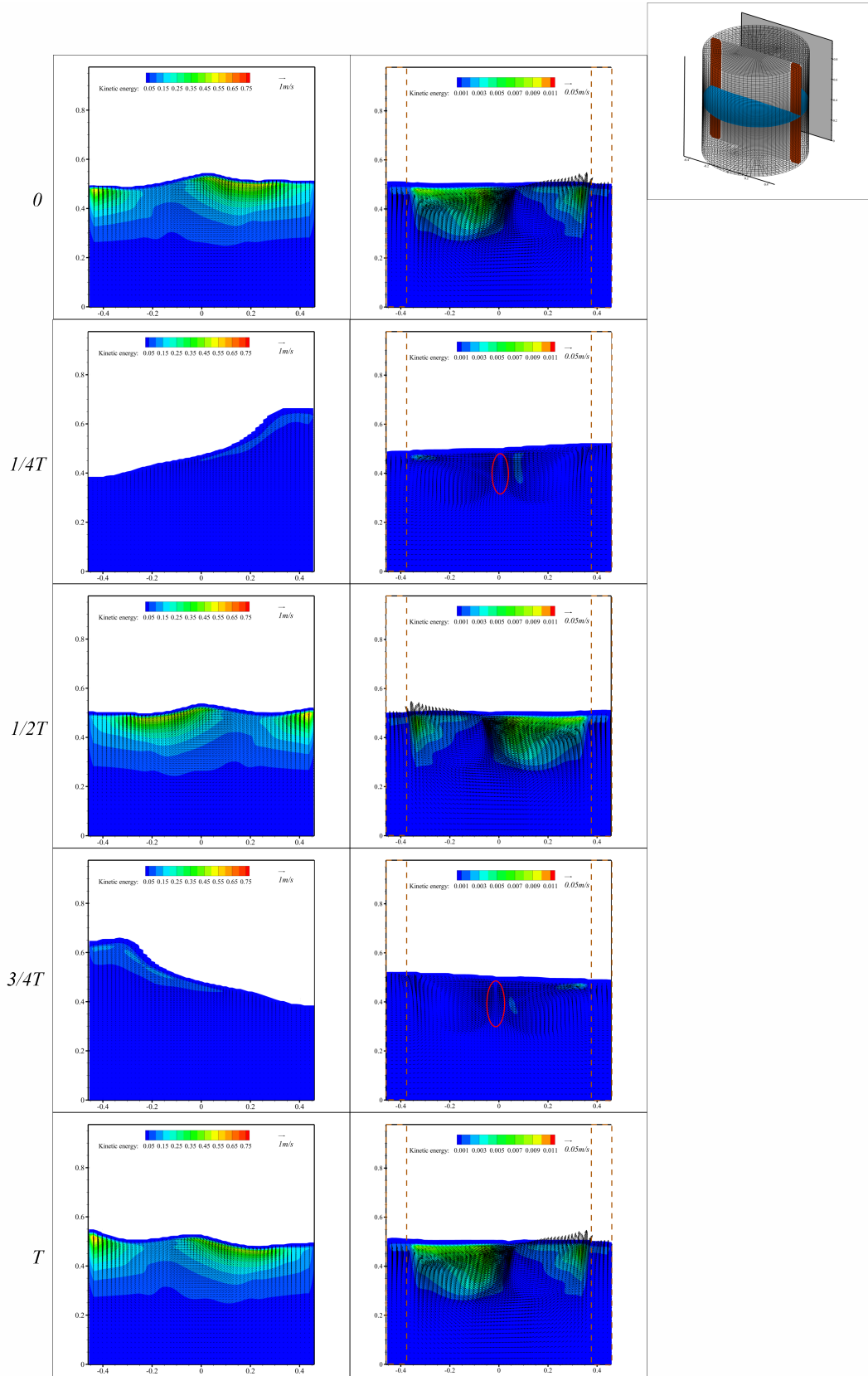


Fig. 18. Kinetic energy distribution and velocity field in y - z slice during one sloshing period in linear sloshing scenario. The location of slice in tank is highlighted in upper right. Left column is free sloshing case. Right column is porous material layer case. Brown dotted region denotes porous material layer.

4.4 Swirling wave mitigation in cylindrical tank

Under an appropriate one-dimensional external forcing, a three-dimensional (3-D) sloshing response can be induced in an upright cylindrical tank, which is known as swirling wave (rotary wave). The induced swirling wave will slam the wall perpendicular to excitation direction, as the pressure probes in free sloshing case measured (Fig. 16). Interestingly, after installing porous material layer inside the cylindrical tank, swirling wave disappeared.

Miles (1984) gave the analytical solutions (Eq. 14), describing the bounds of steady-state wave regime in an upright cylindrical tank (in horizontal harmonic motion). Focusing on the swirling wave induced condition, a series of sloshing test cases are conducted below. According to the steady-state free surface motion (after about 100 periods) and free surface elevation history in two perpendicular directions, 6 test cases (Table 4) are finally classified into planar or swirl wave response categories. It is good to see that numerical results of steady-state wave regimes are consistent with Miles' solutions, as shown in Fig. 19. For planar regime, the sloshing wave stays in two-dimensional, in which the shape of free surface always keeps as a plane. For swirling regime, before entering into steady-state, induced by external excitation, the shape of free surface transforms from a plane into non-planar shape. As non-planar shape develops further, a wave response perpendicular to excitation direction is gradually being induced until finally a steady three-dimensional swirling sloshing wave is established. It is also noted that beyond bound β_4 , due to the robustness of swirling wave, the final steady-state wave response can be either planar or swirl, e.g. case 3 and 6.

$$\frac{A}{R} = \frac{1}{1.684} \left[\frac{(\omega/\omega_1)^2 - 1}{\beta_i} \right]^{3/2} \tag{14}$$

Table 4 Case information on validating swirling wave response.

Basic information	Case	A/R	ω/ω_1
Filling rate $H_1/R=1.5$ $R = 78 \text{ mm}, H = 250$ $\text{mm}, \omega_1 = 15.2$ rad/s	1		0.85
	2	0.0266	1.0
	3		1.1
	4		0.9
	5	0.0133	1.0
	6		1.05

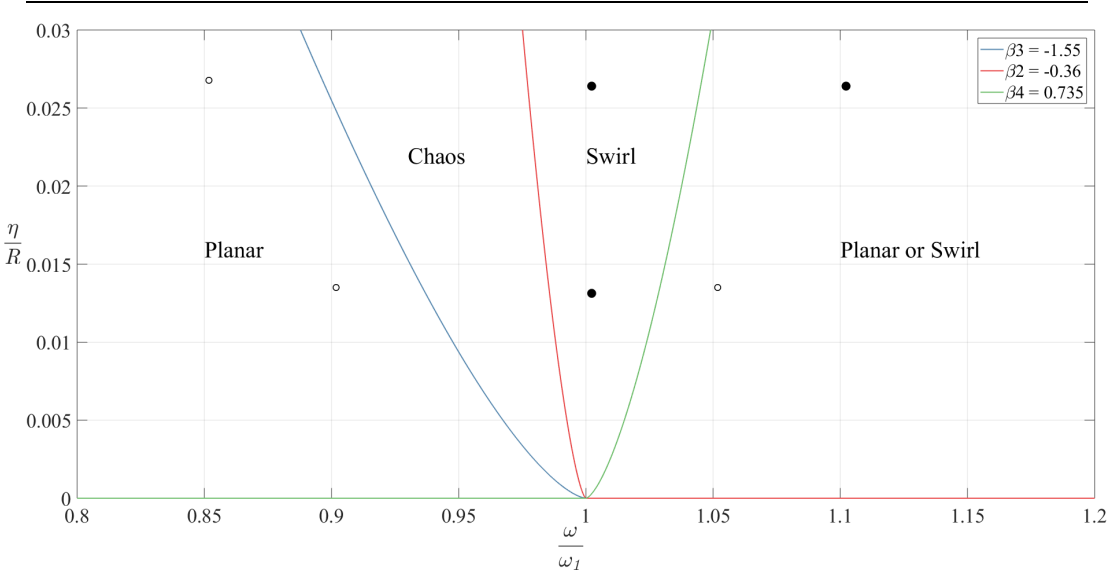


Fig. 19. Steady-state wave sloshing regime diagram in an upright cylindrical tank in terms of different excitation frequency and amplitude. The solid line represents Miles's analytical solution of regime bounds. Circle symbol represents 6 numerical test cases, where open one denotes planar

wave response, closed one denotes swirling wave response.

To investigate the swirling wave response in cylindrical tank with porous material layer, a one-dimensional harmonic excitation in which a steady-state swirling sloshing wave can be induced is chosen according to last section, where $y = A \sin(\omega t)$, $\omega = \omega_1 = 6.16$ rad/s, a large excitation amplitude $A/R = 0.01$ is employed to make the comparison of response amplitude between free sloshing and porous layer case more distinguishable. The setting of porous material layer is consistent with previous linear sloshing case. The swirling wave response is captured by wave height gauges locating at transverse (y) side wall (gauge1) and longitudinal (x) side wall (gauge2).

Fig. 20 gives the measuring free surface evolution in two orthogonal directions. The swirling wave response in free sloshing case is significant and gradually reaches steady state at 50 periods, after which the maximum wave height alternately occurs in two direction, as showed in Fig. 20 (c); After installing porous material layer, the free surface displacement in both sides is suppressed effectively. Meanwhile, the free surface displacement perpendicular to excitation direction (measured at gauge 2) is almost damped to 0, indicating the wave response still stay in planar wave regime. Again, the snapshots in Fig. 21 clearly show that porous material layer effectively prevents the sloshing wave from being inducted into swirling wave, which also means the bounds in sloshing regime diagram has changed after adopting porous layer. The suppressing effect can be explained in energy dissipation perspectives. The inducing of swirling wave regime normally requires much more kinematic energy than planar wave. Besides, the inducing of swirling wave response must undergo periods of non-planar wave response (prominent wave response in chaos regime). With porous material layer, most kinematic energy during sloshing is effectively dissipated. Therefore, the wave response remains as planar wave rather than swirling wave response.

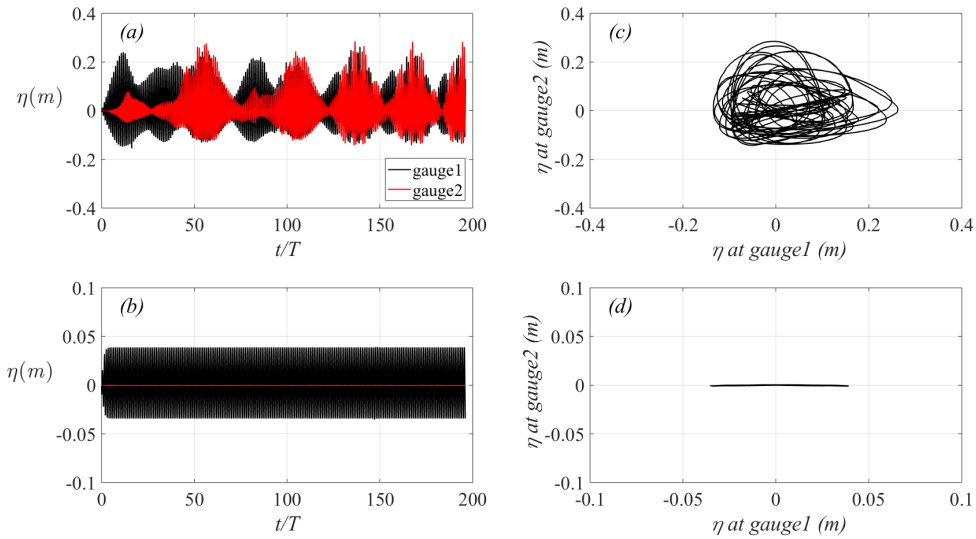


Fig. 20. Comparison of wave free surface displacement evolution near the transverse (y) side wall (gauge1) and longitudinal (x) side wall (gauge2), $T = \frac{2\pi}{\omega_1} \approx 1.02$ s; (a) is free sloshing case, (b) is porous material layer case; right column is the combining comparison of two gauges' measurements.

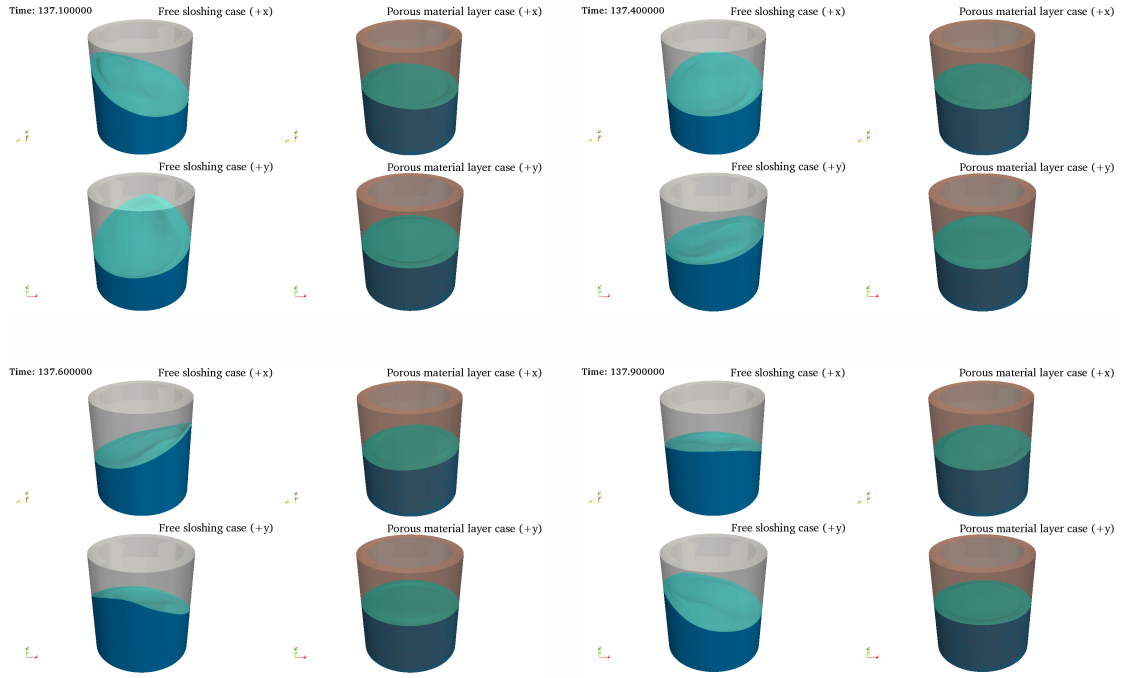


Fig. 21. Snapshots of free surface evolution in one typical sloshing period in nonlinear sloshing scenario, where a steady-state swirling sloshing wave has been established in free sloshing case.

5 Sloshing dampening of porous material layer under seismic excitation

In this section, for the sake of examining the dampening effect of porous material layer in real situation, a real storage tank model with porous layer under seismic excitation is carried out, where the tank size is referred from Fig. 11 without scaling down. Earthquake motions consist of vertical and horizontal components. Above cases only consider horizontal excitation. In fact, during sloshing the vertical earthquake component is considerable important to dynamic sloshing pressure acting on tank wall as indicated in Kang et al. (2019). Based on this conclusion, a three dimension of freedom (DoF) earthquake motion (Fig. 22) is generated from the original motion database (Ancheta et al., 2014). For concisely describing each dimension motion, defining x , y , z direction motions accordingly as longitudinal (EW), transverse (NS), vertical (up-down) motions (Fig. 11). The cylindrical storage tank is taken as almost fully loaded, $H_1/H = 0.9$.

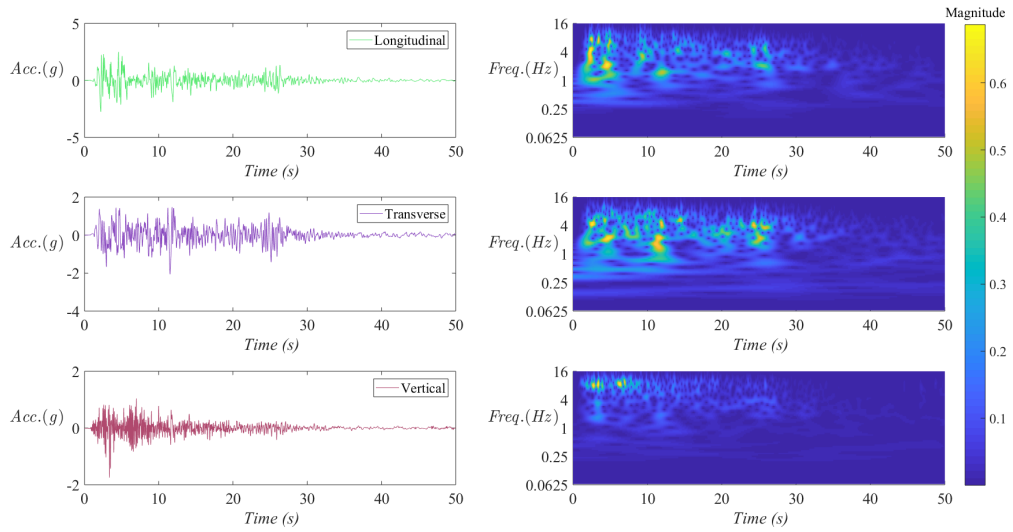


Fig. 22. Three dimensions acceleration history and corresponding wavelet transform.

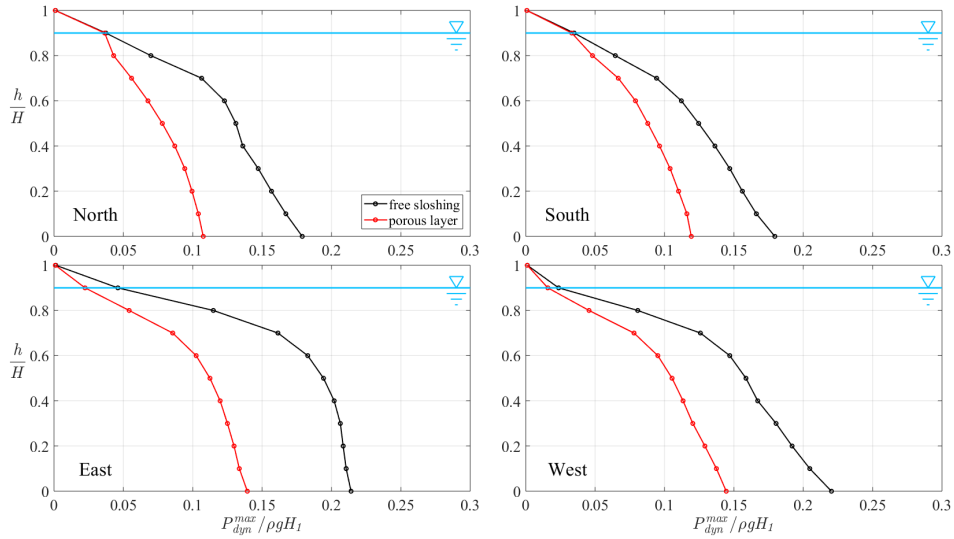


Fig. 23. Comparison of maximum dynamic pressure distribution on four sides wall under EL-centro earthquake excitation.

The maximum dynamic pressure distribution on four sides wall during EL-centro earthquake is presented in Fig. 23. It is noted that when adopting porous material layer, the dynamic pressure is suppressed effectively, especially when closed to tank bottom. Different from the distribution in linear excitation, during EL-centro, the largest maximum dynamic pressure occurs at the tank bottom. Among four sides wall, the maximum pressure all gradually decreases as the vertical height increases. Typically, in the same direction (e.g. east & west) in free sloshing case, the pressure distribution doesn't act the same, indicating nonlinearity during sloshing. But in porous layer case, in the same direction, the pressure distribution is almost identical.

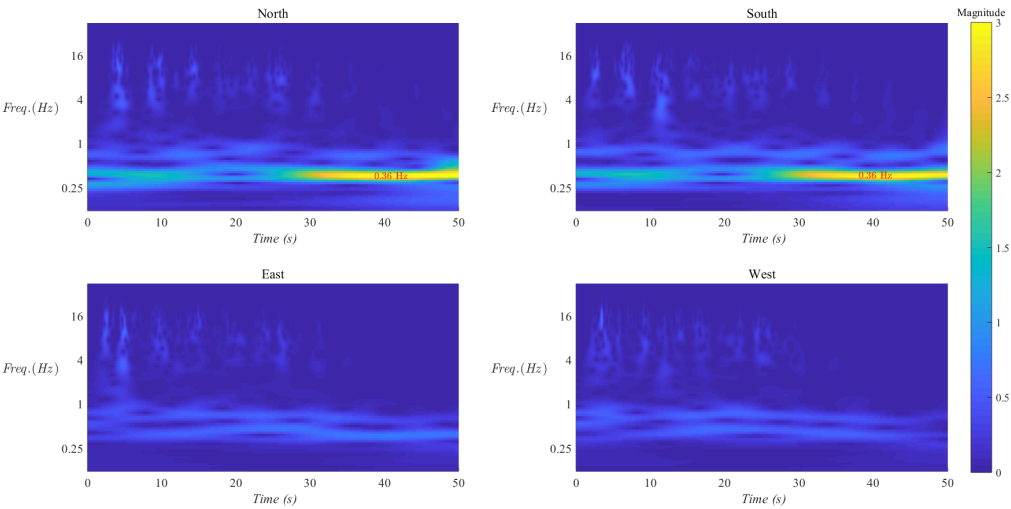


Fig. 24. Wavelet transform of dynamic pressure near free surface of four sides wall (free sloshing case).

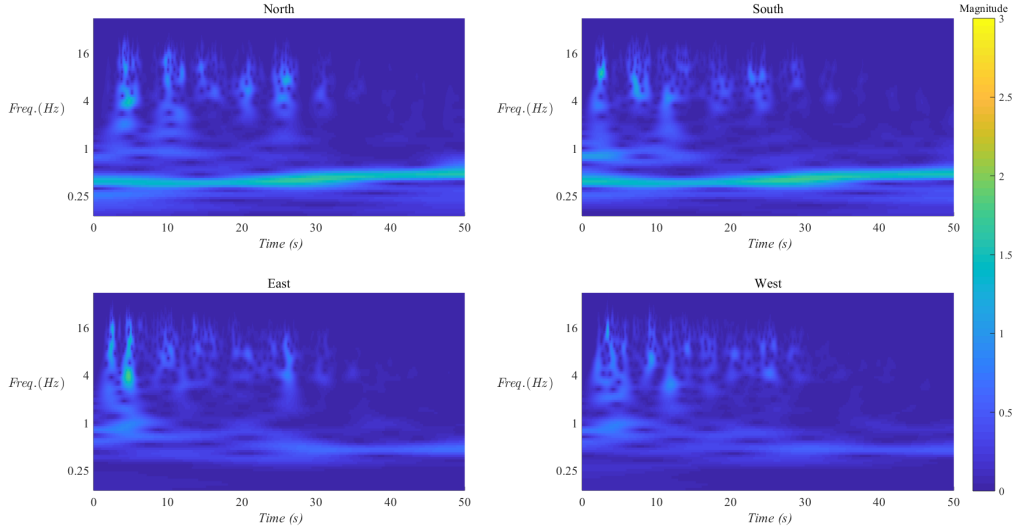


Fig. 25. Wavelet transform of dynamic pressure near free surface of four sides wall (porous layer case).

Finally, wavelet transform is applied for analyzing the dynamic pressure near free surface ($H_1/H = 0.9$) at four sides. In free sloshing case (Fig. 24), the separated frequency components at the same direction are identical. Typically, along transverse direction (north & south), one dominant frequency ridge is found ($f = 0.36$ Hz). Except dominant component, several impulsive frequencies occur in high frequency domain, while only lasting for a short time. After adopting porous layer (Fig. 25), along transverse direction, the magnitude of previous dominant frequency has been reduced. While along longitudinal direction, no significant change has found among spectrograms. Overall, it is great to see adopting porous layer effectively mitigate the severe impact load around a cylindrical tank inner wall when a real earthquake happens.

6 Conclusions

In this study, which is focused on sloshing mitigation in cylindrical tanks, a novel approach by attaching porous material layer to interior tank wall is proposed and its effectiveness is numerically investigated with the aid of open source CFD code OpenFOAM. By comparing free surface displacement and dynamic pressure with available data from the literature, four validation cases including mesh convergence tests are simulated respectively and these include liquid sloshing in 3-D cylindrical tank with and without ring baffles, Darcy seepage experiment on flowing through porous material, porous dam break. Fair agreements are obtained. To reveal the damping effect of porous material layer, the response of free surface displacement and dynamic pressure are examined under 1-D linear sloshing, 1-D nonlinear sloshing and 3-D EL-centro earthquake. Time-frequency wavelet transform, kinetic energy evolution and maximum dynamic pressure distribution along tank wall are presented and the effects of porous material layer are analysed. Noteworthy phenomena and conclusions are drawn as follows:

(1) Under 1-D excitation (linear sloshing): When installing porous material layer, the previous strong kinetic energy occurs inside porous layer is suppressed effectively, indicating that the inner friction of porous layer plays a prominent role on dissipating kinetic energy; For installing porous material layer case, the response phase of part fluid lags, which resulting in flow collision at the center fluid column of cylindrical tank; The largest maximum dynamic pressure along tank wall occurs near the free surface; In free sloshing case, distinguished dynamic pressure response is captured along the side tank wall perpendicular to excitation direction, indicating that 3-D swirling

wave is induced. After installing porous material layer, this 3-D response is suppressed effectively. Moreover, the dampening effect of porous material layer also performs well in other frequency range in linear sloshing scenario. It is noted that under resonant frequency, the sloshing damping effect is most prominent.

(2) Under 1-D excitation (nonlinear sloshing): Distinguished steady-state swirling wave response is well captured within the bounds β_2 and β_4 . While beyond β_4 , swirling wave response is still possible be induced in certain situation; The significant swirling wave response is showed in free sloshing case, while adopting porous material layer, steady-state wave response keeps as planar wave, indicating the effect of porous material layer on suppressing swirling wave response.

(3) Under EL-centro excitation (complicated 3DoF excitation): The largest maximum dynamic pressure along tank wall is found near the tank bottom, diminishing gradually as height increases; For porous material layer case, the maximum dynamic pressure along tank wall is mitigated effectively. Also, pressure distribution discrepancy along the same direction is eliminated; The magnitude of original dominant frequency components (0.36 Hz) in free sloshing case is suppressed significantly when installing porous material layer.

From this study, sloshing damping effect of porous material layer is found to be significant under different excitation situations, which can be essentially attributed to intrinsic friction of porous material itself and the results show promise of this new technique being applied in future LPG storage tank design.

CRedit authorship contribution statement

Mi-An Xue: Conceptualization, Methodology, Writing - original draft, Writing - review & editing. **Zhouyu Jiang:** Investigation, Writing - original draft. **Pengzhi Lin:** Supervision. **Jinhai Zheng:** Resources. **Xiaoli Yuan:** Project administration. **Ling Qian:** Writing - review & editing.

Declaration of competing interest

The authors declare that they have no known competing financial interests or personal relationships that could have appeared to influence the work reported in this paper.

Acknowledgement

The study is supported by the Fundamental Research Funds for the Central Universities (B200202055), the National Natural Science Foundation of China (51679079), and Key Laboratory of Ministry of Education for Coastal Disaster and Protection, Hohai University (202005).

Reference

- Akyldz, H., Erdem Unal, N., Aksoy, H. 2013, An experimental investigation of the effects of the ring baffles on liquid sloshing in a rigid cylindrical tank. *Ocean Eng.* 59, 190-197.
- Ancheta, T.D., Darragh, R.B., Stewart, J.P., Seyhan, E., Silva, W.J., Chiou, B.S.J., Wooddell, K.E., Graves, R.W., Kottke, A.R., Boore, D.M., Kishida, T., Donahue, J.L. 2014, NGA-West2 Database. *Earthq. Spectra* 30, 989-1005.
- Biswal, K.C., Bhattacharyya, S.K., Sinha, P.K. 2006, Non-linear sloshing in partially liquid filled containers with baffles. *Int. J. Numer. Methods Eng.* 68, 317-337.
- Bouvard, J., Herreman, W., Moisy, F. 2017, Mean mass transport in an orbitally shaken cylindrical container. *Phys. Rev. Fluids* 2, 084801.
- Caron, P.A., Cruchaga, M.A., Larreteguy, A.E. 2018, Study of 3D sloshing in a vertical cylindrical tank. *Phys. Fluids* 30, 082112.

- Chen, Y., Xue, M.-A. 2018, Numerical simulation of liquid sloshing with different filling levels using OpenFOAM and experimental validation. *Water* 10, 1752.4
- Cho, I.H. 2021, Liquid sloshing in a swaying/rolling rectangular tank with a flexible porous elastic baffle. *Mar. Struct.* 75, 102865.
- del Jesus, M., Lara, J.L., Losada, I.J. 2012, Three-dimensional interaction of waves and porous coastal structures. Part I: Numerical model formulation. *Coastal Eng.* 64, 57-72.
- Faller, A.J. 2001, The constant- V vortex. *J. Fluid Mech.* 434, 167-180.
- Faltinsen, O.M., Timokha, A.N. 2019, An inviscid analysis of the Prandtl azimuthal mass transport during swirl-type sloshing. *J. Fluid Mech.* 865, 884-903.
- Funakoshi, M., Inoue, S. 1988, Surface waves due to resonant horizontal oscillation. *J. Fluid Mech.* 192, 219-247.
- Gomez-Goni, J., Garrido-Mendoza, C.A., Luis Cercos, J., Gonzalez, L. 2013, Two phase analysis of sloshing in a rectangular container with Volume of Fluid (VOF) methods. *Ocean Eng.* 73, 208-212.
- Haroun, M.A. 1983, Vibration studies and tests of liquid storage tanks. *Earthq. Eng. Struct. Dyn.* 11, 179-206.
- Hernandez-Hernandez, D., Larkin, T., Chouw, N., Banide, Y. 2020, Experimental findings of the suppression of rotary sloshing on the dynamic response of a liquid storage tank. *J. Fluids Struct.* 96, 103007.
- Higuera, P., Lara, J.L., Losada, I.J. 2014a, Three-dimensional interaction of waves and porous coastal structures using OpenFOAM. Part I: Formulation and validation. *Coastal Eng.* 83, 243-258.
- Higuera, P., Lara, J.L., Losada, I.J. 2014b, Three-dimensional interaction of waves and porous coastal structures using OpenFOAM. Part II: Application. *Coastal Eng.* 83, 259-270.
- Hirt, C.W., Nichols, B.D. 1981, Volume of fluid (VOF) method for the dynamics of free boundaries. *J. Comput. Phys.* 39, 201-225.
- Hsu, T.-J., Sakakiyama, T., Liu, P.L.F. 2002, A numerical model for wave motions and turbulence flows in front of a composite breakwater. *Coastal Eng.* 46, 25-50.
- Hutton, R.E. 1963, An investigation of resonant, nonlinear, nonplanar free surface oscillations of a fluid. NASA-TN-D-1870.
- Iranmanesh, A., Passandideh-Fard, M. 2017, A 2D numerical study on suppressing liquid sloshing using a submerged cylinder. *Ocean Eng.* 138, 55-72.
- Kang, T.-W., Yang, H.-I., Jeon, J.-S. 2019, Earthquake-induced sloshing effects on the hydrodynamic pressure response of rigid cylindrical liquid storage tanks using CFD simulation. *Eng. Struct.* 197, 109376.
- Koh, C.G., Luo, M., Gao, M., Bai, W. 2013, Modelling of liquid sloshing with constrained floating baffle. *Comput. Struct.* 122, 270-279.
- Liang, H., Santo, H., Shao, Y., Law, Y.Z., Chan, E.S. 2020, Liquid sloshing in an upright circular tank under periodic and transient excitations. *Phys. Rev. Fluids* 5, 084801.
- Lin, P. 2007, A fixed-grid model for simulation of a moving body in free surface flows. *Comput. Fluids* 36, 549-561.
- Lin, P., Cheng, L., Liu, D. 2016, A two-phase flow model for wave-structure interaction using a virtual boundary force method. *Comput. Fluids* 129, 101-110.
- Liu, P.L.F., Lin, P., Chang, K.-A., Sakakiyama, T. 1999, Numerical modeling of wave interaction with porous structures. *J. Waterw. Port Coast. Ocean Eng.* 125, 322-330.
- Miles, J.W. 1984, Resonantly forced surface waves in a circular cylinder. *J. Fluid Mech.* 149, 15-31.
- Molin, B. 2011, Hydrodynamic modeling of perforated structures. *Appl. Ocean Res.* 33, 1-11.
- Molin, B., Remy, F. 2013, Experimental and numerical study of the sloshing motion in a rectangular tank with a perforated screen. *J. Fluids Struct.* 43, 463-480.

- Ning, D., Su, P., Zhang, C. 2019, Experimental Study on A Sloshing Mitigation Concept Using Floating Layers of Solid Foam Elements. *China Ocean Eng.* 33, 34-43.
- Peng, C., Xu, G., Wu, W., Yu, H.-S., Wang, C. 2017, Multiphase SPH modeling of free surface flow in porous media with variable porosity. *Comput. Geotech.* 81, 239-248.
- Polubarinova-Kochina, P.Y. 1962, *Theory of Groundwater Movement*. Princeton University Press, Princeton, N.J.
- Prandtl, L. 1949, Erzeugung von Zirkulationen beim Schütteln von Gefäßen. *Z. Angew. Math. Mech* 29, 8-9.
- Royon-Lebeaud, A., Hopfinger, E.J., Cartellier, A. 2007, Liquid sloshing and wave breaking in circular and square-base cylindrical containers. *J. Fluid Mech.* 577, 467-494.
- Unal, U.O., Bilici, G., Akyildiz, H. 2019, Liquid sloshing in a two-dimensional rectangular tank: A numerical investigation with a T-shaped baffle. *Ocean Eng.* 187, 106183.
- Van Gent, M.R.A. 1995, Wave interaction with permeable coastal structures. PhD Thesis. Delft University of Technology, Delft, The Netherlands.
- Waterhouse, D.D. 1994, Resonant sloshing near a critical depth. *J. Fluid Mech.* 281, 313-318.
- Xue, M.-A., Lin, P. 2011, Numerical study of ring baffle effects on reducing violent liquid sloshing. *Comput. Fluids* 52, 116-129.
- Xue, M.-A., Lin, P., Zheng, J., Ma, Y., Yuan, X., Nguyen, V.-T. 2013, Effects of perforated baffle on reducing sloshing in rectangular tank: Experimental and numerical study. *China Ocean Eng.* 27, 615-628.
- Xue, M.-A., Zheng, J., Lin, P., Yuan, X. 2017, Experimental study on vertical baffles of different configurations in suppressing sloshing pressure. *Ocean Eng.* 136, 178-189.
- Xue, M.-A., Chen, Y., Zheng, J., Qian, L., Yuan, X. 2019, Fluid dynamics analysis of sloshing pressure distribution in storage vessels of different shapes. *Ocean Eng.* 192, 106582.
- Xue, M.-A., Kargbo, O., Zheng, J. 2020a, Seiche oscillations of layered fluids in a closed rectangular tank with wave damping mechanism. *Ocean Eng.* 196, 106842.
- Xue, M.-A., Jiang, Z., Hu, Y.-A., Yuan, X. 2020b, Numerical study of porous material layer effects on mitigating sloshing in a membrane LNG tank. *Ocean Eng.* 218, 108240.
- Ye, W., Liu, J., Lin, G., Zhou, Y., Yu, L. 2018, High performance analysis of lateral sloshing response in vertical cylinders with dual circular or arc-shaped porous structures. *Appl. Ocean Res.* 81, 47-71.
- Yu, L., Xue, M.-A., Zheng, J. 2019, Experimental study of vertical slat screens effects on reducing shallow water sloshing in a tank under horizontal excitation with a wide frequency range. *Ocean Eng.* 173, 131-141.
- Zhang, C., Su, P., Ning, D. 2019a, Hydrodynamic study of an anti-sloshing technique using floating foams. *Ocean Eng.* 175, 62-70.
- Zhang, X., Huang, H., Song, X. 2019b, On natural frequencies and modal shapes in two-dimensional asymmetric and symmetric moonpools in finite water depth. *Appl. Ocean Res.* 82, 117-129.